Separation Science and Technology
Publication details, including instructions for authors and subscription information:
http://www.informaworld.com/smpp/title~content=t713708471

Analysis of the Salt Retention of Nanofiltration Membranes Using the Donnan-Steric Partitioning Pore Model

Johan Schaep[a]; Carlo Vandecasteele[a]; A. Wahab Mohammad[b]; W. Richard Bowen[b]
[a] DEPARTMENT OF CHEMICAL ENGINEERING, UNIVERSITY OF LEUVEN, HEVERLEE, BELGIUM
[b] DEPARTMENT OF CHEMICAL AND BIOLOGICAL PROCESS ENGINEERING, UNIVERSITY OF WALES SWANSEA, SWANSEA, UNITED KINGDOM

Online publication date: 20 October 1999

To cite this Article Schaep, Johan , Vandecasteele, Carlo , Mohammad, A. Wahab and Bowen, W. Richard(1999) 'Analysis of the Salt Retention of Nanofiltration Membranes Using the Donnan-Steric Partitioning Pore Model', Separation Science and Technology, 34: 15, 3009 — 3030
To link to this Article: DOI: 10.1081/SS-100100819
URL: http://dx.doi.org/10.1081/SS-100100819

SEPARATION SCIENCE AND TECHNOLOGY, **34**(15), pp. 3009–3030, 1999

Analysis of the Salt Retention of Nanofiltration Membranes Using the Donnan–Steric Partitioning Pore Model

JOHAN SCHAEP* and CARLO VANDECASTEELE
DEPARTMENT OF CHEMICAL ENGINEERING
UNIVERSITY OF LEUVEN
W. DE CROYLAAN 46, B-3001 HEVERLEE, BELGIUM

A. WAHAB MOHAMMAD and W. RICHARD BOWEN
CENTRE FOR COMPLEX FLUIDS PROCESSING
DEPARTMENT OF CHEMICAL AND BIOLOGICAL PROCESS ENGINEERING
UNIVERSITY OF WALES SWANSEA
SWANSEA SA2 8PP, UNITED KINGDOM

ABSTRACT

The performance of four commercial nanofiltration membranes was analyzed by the Donnan–steric partitioning pore model (DSPM) that describes solute transport through a membrane using the extended Nernst–Planck equation. Retention measurements were carried out as a function of the permeate flux for uncharged solutes, which allowed characterization of the membranes in terms of an effective membrane pore radius and the ratio of an effective membrane thickness to the porosity. Retention measurements with single salt solutions of NaCl, Na_2SO_4, $MgCl_2$, and $MgSO_4$ clearly showed the effect of ion concentration and ion valence on the retention. The DSPM model was used to evaluate the effective membrane charge density by analyzing the retention of single salt solutions. The analysis showed that the charge density is not constant but depends very much on the salt and its concentration. This is attributed to ion adsorption on the membrane material. For magnesium salts this could lead to a positive membrane charge. This phenomenon was found for each of the membrane materials.

Key Words. Nanofiltration; Nernst–Planck equation; Salt solutions; Membrane charge; Retention

* To whom correspondence should be addressed. Telephone: +32 16 322340. FAX: +32 16 322991. E-mail: johan.schaep@cit.kuleuven.ac.be

INTRODUCTION

Applications of nanofiltration are increasing rapidly in several areas, e.g., drinking water production, dairy industry, and the paper industry. Nevertheless, the mechanism of transport through these membranes has not yet been fully understood (1).

Most authors agree that the pore size and the charge density of nanofiltration membranes are the main parameters that determine the extent to which solutes are rejected. A third parameter, the membrane thickness, determines the hydrodynamic resistance and consequently the flux through the membrane. If these membrane characteristics are known and the effect on solute transport can be described, the membrane performance can be quantified.

Most techniques used in ultrafiltration cannot be applied to determine the pore size of nanofiltration membranes experimentally because of the small pore dimensions. Atomic force microscopy (AFM) is a useful technique to analyze the membrane surface, and hence to determine the pore size distribution. However, the size determined in this way is not necessarily a useful parameter to characterize filtration performance because not only are the surface characteristics of a pore important but also the total pore shape from the feed to the permeate side. The membrane charge density can be evaluated in a number of ways, of which electrokinetic measurements (determination of zeta potential), membrane potential measurements, and measurements of ion-exchange capacities (to obtain the number of charged groups in the membrane) are the most important. These methods can be used to give more insight into the rejection performance of a membrane, but so far they give only qualitative information. Electron microscopy can be used to determine the membrane thickness, but the support layer can also influence the transport to a significant extent (2). Another way to characterize a nanofiltration membrane is by solute rejection measurements. A model is then applied to deduce the membrane characteristics of interest.

Much effort was devoted for several years to developing models appropriate for nanofiltration. One such model was developed by Bowen et al. (3, 4). The so-called Donnan–steric partitioning pore model (DSPM) is based on the extended Nernst–Planck equation. It assumes the membrane is porous, and size effects are taken into account by incorporating steric hindrance factors. In contrast with a space-charge model (5), the radial distribution of the potential over the membrane pore is considered constant. The model has been applied to the PES 5 membrane (3, 4). After characterization of the membrane in terms of an effective pore radius, the ratio of an effective membrane thickness to the porosity, and an effective membrane charge density using uncharged solutes and single salt solutions, the retention for a mixture of $NaCl/Na_2SO_4$ was adequately predicted. The model was also successful in predicting the perfor-

mance of the CA30 nanofiltration membrane for a dye/salt solution (6).

In the present paper the DSPM model is used to analyze the performance of four nanofiltration membranes, each with a different membrane structure and with different salt retention properties. Besides the retention of NaCl and Na_2SO_4 solutions, the retention of $MgCl_2$ and $MgSO_4$ solutions is also studied.

THEORETICAL BACKGROUND (3)

The transport of solutes inside the membranes can be described by the extended Nernst–Planck equation:

$$j_i = -D_{i,p}\frac{dc_i}{dx} - \frac{z_i c_i D_{i,p}}{RT} F \frac{d\psi}{dx} + K_{i,c} c_i V \tag{1}$$

where

$$D_{i,p} = K_{i,d} D_{i,\infty} \tag{2}$$

j_i is the flux of solute i, and the terms on the right hand side represent transport due to diffusion, electric field gradient, and convection, respectively (see List of Symbols for definitions). The hindered nature of diffusion and convection of the ions inside the membrane are accounted for by the factors $K_{i,d}$ and $K_{i,c}$.

The hindrance factors, $K_{i,d}$ and $K_{i,c}$, are a function of λ, the ratio of the solute radius to the pore radius, and are related to the hydrodynamic coefficients K^{-1}, the enhanced drag, and G, the lag coefficient, of a spherical solute moving inside a cylindrical pore of infinite length. The enhanced drag and the lag coefficients were calculated using the finite-element technique and a centerline approach (7):

$$K^{-1}(\lambda, 0) = 1.0 - 2.30\lambda + 1.154\lambda^2 + 0.224\lambda^3 \tag{3}$$

$$G(\lambda, 0) = 1.0 + 0.054\lambda - 0.988\lambda^2 + 0.441\lambda^3 \tag{4}$$

Assuming that the solute velocity is fully developed inside the pore and has a parabolic profile of the Hagen–Poiseuille type, the hindrance factors become (8):

$$K_{i,d} = K^{-1}(\lambda, 0), \qquad K_{i,c} = (2 - \phi)\, G(\lambda, 0) \tag{5}$$

where the steric term, ϕ, is given by

$$\phi = (1 - \lambda)^2 \tag{6}$$

and accounts for the finite size of the solute.

MARCEL DEKKER, INC.
270 Madison Avenue, New York, New York 10016

Uncharged Solutes

For uncharged solutes, only the diffusive and convective flows affect the transport of solutes inside the membrane. The solute flux can thus be expressed as

$$j_i = -D_{i,p}\frac{dc_i}{dx} + K_{i,c}c_iV \tag{7}$$

All variables are defined in terms of radially averaged quantities.

In order to obtain an expression for the rejection of the solute, Eq. (7) is integrated across the membrane. The solute concentrations in the membrane at the upper ($x = 0$) and lower ($x = \Delta x$) surfaces are expressed in terms of the external concentrations ($C_{i,m}$ and $C_{i,p}$) using the equilibrium partition coefficient ϕ:

$$\phi = \frac{c_{i,x=0}}{C_{i,m}} = \frac{c_{i,x=\Delta x}}{C_{i,p}} \tag{8}$$

For purely steric interactions between the solute and the pore wall, ϕ is the same as given in Eq. (6).

In terms of rejection, Eq. (7) becomes

$$R = 1 - \frac{C_{i,p}}{C_{i,m}} = 1 - \frac{K_{i,c}\phi}{1 - \exp(-\mathrm{Pe}_m)[1 - \phi K_{i,c}]} \tag{9}$$

where the Peclet number, Pe_m, is defined as:

$$\mathrm{Pe}_m = \frac{K_{i,c}}{K_{i,d}}\frac{J_v\Delta x}{D_{i,\infty}A_k} \tag{10}$$

The rejection at a given filtration flux J_v, is thus a function of two parameters, λ and $\Delta x/A_k$. Equations (9) and (10) show that retention increases with the filtration flux and that it reaches a value of $1 - \phi K_{i,c}$ at infinite filtration flux.

The Hagen–Poiseuille equation gives the relationship between the pure water flux and the applied pressure across the membrane:

$$J_w = \frac{r_p^2\Delta P}{8\mu(\Delta x/A_k)} \tag{11}$$

If r_p is known, the value for $\Delta x/A_k$ can be calculated. This independently determined value of $\Delta x/A_k$ can be compared to $\Delta x/A_k$ obtained from the fitting of the rejection data.

Charged Solutes

The conditions for electroneutrality in the bulk solution and inside the membranes are expressed respectively as

$$\sum_{i=1}^{n} z_iC_i^0 = 0, \qquad \sum_{i=1}^{n} z_ic_i = -X \tag{12}$$

MARCEL DEKKER, INC.
270 Madison Avenue, New York, New York 10016

where C_i^0 is the bulk concentration of ion i, c_i is the concentration of ion i inside the membrane, and X is the effective volumetric membrane charge density. X is assumed constant at all points in the active part of the membrane. The zero current condition inside the membrane is expressed as

$$I_c = \sum_{i=1}^{n} F(z_i j_i) = 0 \tag{13}$$

Since the electric potential gradient is the same for every ion inside the membrane, the electric potential and concentration gradients can be derived from Eq. (1). By rearranging Eq. (1), the concentration gradient may be written as

$$\frac{dc_i}{dx} = \frac{J_v}{D_{i,p}A_k}(K_{i,c}c_i - C_{i,p}) - \frac{z_i c_i}{RT} F \frac{d\psi}{dx} \tag{14}$$

where the flux j_i is expressed as

$$j_i = J_v C_{i,p}/A_k \tag{15}$$

Similarly, the potential gradient term can be expressed as

$$\frac{d\psi}{dx} = \frac{\sum_{i=1}^{n} \frac{z_i J_v}{D_{i,p}A_k}(K_{i,c}c_i - C_{i,p})}{\frac{F}{RT}\sum_{i=1}^{n}(z_i^2 c_i)} \tag{16}$$

Equations (14) and (16) can be solved by using the following boundary conditions together with the equations for electroneutrality (12):

$$\begin{aligned} &\text{at } x = 0: && C_i^0 = C_{i,m} \\ &\text{at } x = \Delta x: && C_i^0 = C_{i,p} \end{aligned} \tag{17}$$

where $C_{i,m}$ and $C_{i,p}$ are the feed and permeate concentrations of ion i at the interfaces of the membrane, respectively, i.e., the concentrations just outside the membrane.

The concentration at the interface (i.e., just inside the membrane) can be determined using the following equilibrium conditions which will be taken as a combination of the Donnan and steric effects:

$$\frac{c_i}{C_i^0} = \phi \exp\left(-\frac{z_i F}{RT}\Delta\psi_D\right) \tag{18}$$

The term ϕ is the steric partitioning term which accounts for the steric effects at the entrance of the membrane, and is given by Eq. (6). The equations were solved numerically using the Runge–Kutta–Gill method.

MARCEL DEKKER, INC.
270 Madison Avenue, New York, New York 10016

All fluxes, concentrations, potentials, and velocities are defined in terms of radially averaged quantities, so that no radial distributions are taken into account. Nonidealities of properties inside the membrane as a result of coupling between ions and ions, or ions and membrane, are assumed to be accounted for by the effective membrane charge density. Also, the ion distribution between the bulk solution and the pore may be influenced by a change of the dielectric constant of the solvent going from the solution to the membrane phase. It has often been discussed in the literature that the dielectric constant in narrow pores may be lower than in the bulk, but a quantitative description is not available (9, 10). Here, solvent dielectric effects on ion partitioning are not taken into account.

EXPERIMENTAL

Membranes

Flat sheet samples of four commercially available nanofiltration membranes were used. Some characteristics are given in Table 1. The NF40 and UTC20 membranes have a low molecular weight cutoff (MWCO) value.

Information about the charge of nanofiltration membranes is not always available but is an important characteristic in interpretation of salt retention. Sulfonated polyethersulfone membranes (such as NTR7450) carry a negative charge. Membranes made from cellulose acetate (such as CA30) are supposed to be negatively charged (11). The charge of polyamide membranes can be either negative or positive. For NF40 the membrane is negatively charged according to some publications (1, 12–14). For the UTC20 membrane the information in the literature is contradictory: Raman et al. (1) state the membrane is negative, Simons (12) states the membrane is amphoteric and negatively charged at neutral pH, and according to information from the manufacturer

TABLE 1
Membranes Used

Membrane	Manufacturer	Membrane material	MWCO (estimate)	Charge (at neutral pH)
NTR7450	Nitto Denko	Sulfonated polyethersulfone	600–800	Negative
CA30	Hoechst	Cellulose acetate	1000	Negative
NF40	Dow	Polypiperazine amide	180	Negative
UTC20	Toray Industries	Polypiperazine amide	350	?

UTC20 is positively charged. The charge density can also be determined from measurements of the membrane potential: the charge of the UTC20 membrane is found to be positive while NTR7450, CA30, and NF40 are negatively charged membranes (15).

Measurements of the membrane charge density are not directly used in the model as the values obtained for the fixed charge density of the membranes are only qualitative in general (11).

Equipment

Experiments were carried out in a laboratory-scale test cell (Amafilter). A schematic diagram of the apparatus is presented in Ref. 16. All experiments were carried out at a cross-flow velocity of 6 m/s and at a constant temperature of 25°C, using a cross-flow filtration cell with a rectangular flow channel (equivalent hydraulic diameter $d_h = 4.2$ mm, total length of flow channel = 293 mm) and an effective membrane area of 44 cm^2.

Concentration polarization was taken into account for all experimental results. The correlation of Dittus and Boelter for turbulent flow in channels was used to calculate the mass transfer coefficient k in the boundary layer, related to the Sherwood number (17):

$$\mathrm{Sh} = \frac{kd_h}{D_{\mathrm{eff}}} = 0.023\mathrm{Re}^{0.8}\mathrm{Sc}^{0.33} \tag{19}$$

where D_{eff} for a salt is calculated as (18)

$$D_{\mathrm{eff}} = \frac{D_+D_-(z_+ - z_-)}{z_+D_+ - z_-D_-} \tag{20}$$

The real solute retention, i.e., the retention corrected for concentration polarization, was calculated by using the film model (2), and will be used further in the text.

Membrane Characterization

Ultrapure water (Milli-Q system of Millipore) was used to measure the pure water flux at different transmembrane pressures to determine the pure water permeability of the membranes.

Solutions of galactose (molar mass = 180 g/mol), maltose (342 g/mol), and raffinose (504 g/mol) at a concentration of 500 mg/L were filtered. Retentions were measured as a function of the permeate flux by varying the transmembrane pressure from 3.5 to 20 bar. The experiments were carried out at pH 5.5–6. For the analysis of the saccharide solutions a colorimetric method based on a treatment with phenol and sulfuric acid was used (19).

MARCEL DEKKER, INC.
270 Madison Avenue, New York, New York 10016

Single Salt Solutions

The retention of single salt solutions (NaCl, Na_2SO_4, $MgCl_2$, and $MgSO_4$) was determined as a function of the permeate flux at different feed concentrations. For the CA30 membrane the concentration range was 0.010–0.200 eq/L; for the other membranes 0.050–0.750 eq/L. Feed and permeate samples were analyzed by conductivity measurements. All solutes were prepared using Milli-Q water and analytical grade salts. The experiments were carried out at pH 5.5–6.

RESULTS AND DISCUSSION

Membrane Characterization

Table 2 gives the pure water permeability for four nanofiltration membranes. For both NTR7450 and UTC20 the permeabilities are rather high, while for CA30 and NF40 values common for nanofiltration membranes [1.4–12 L/(hm^2·bar)] were obtained (2). The last column of Table 2 gives the value for $r_p^2/(\Delta x/A_k)$, calculated from the Hagen–Poiseuille equation (Eq. 11).

Experimental data for uncharged solutes are shown for the CA30 and NTR7450 membranes in Figs. 1 and 2, respectively. The retention of the saccharides increases as the flux increases. Much higher retentions were found for NF40 and UTC20: galactose was retained to about 95% by both membranes; maltose and raffinose were completely retained. The experimental points were fitted well by Eqs. (9) and (10), as shown by the full lines in Figs. 1 and 2. Two membrane characteristics were deduced from these curves: the effective membrane pore radius and the ratio of the effective membrane thickness to the porosity. The criteria for the best fit was a minimization of the least-squares deviation. The results are shown in Table 3.

The deduced effective membrane pore radius was 0.94 ± 0.01 nm (mean ± standard deviation for the three saccharides) for CA30 and 0.69 ± 0.13 nm for

TABLE 2
Pure Water Permeability Data of the Membranes Used

Membrane	Pure water permeability [L/(hm^2·bar)]	$r_p^2/(\Delta x/A_k)$ (10^{-13} m)
NTR7450	23.2	4.6
CA30	6.5	1.3
NF40	9.4	1.9
UTC20	25.0	5.0

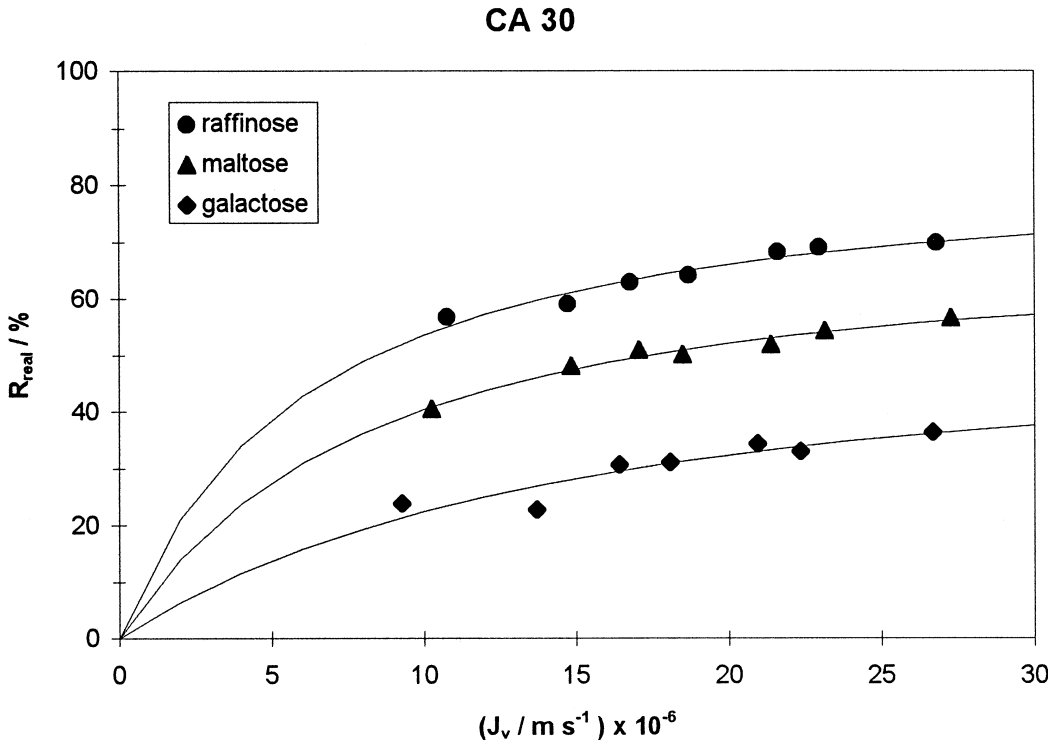

FIG. 1 The retention of three saccharides as a function of the permeate flux for the CA30 membrane. The full lines are the result of a best fit using Eqs. (9) and (10).

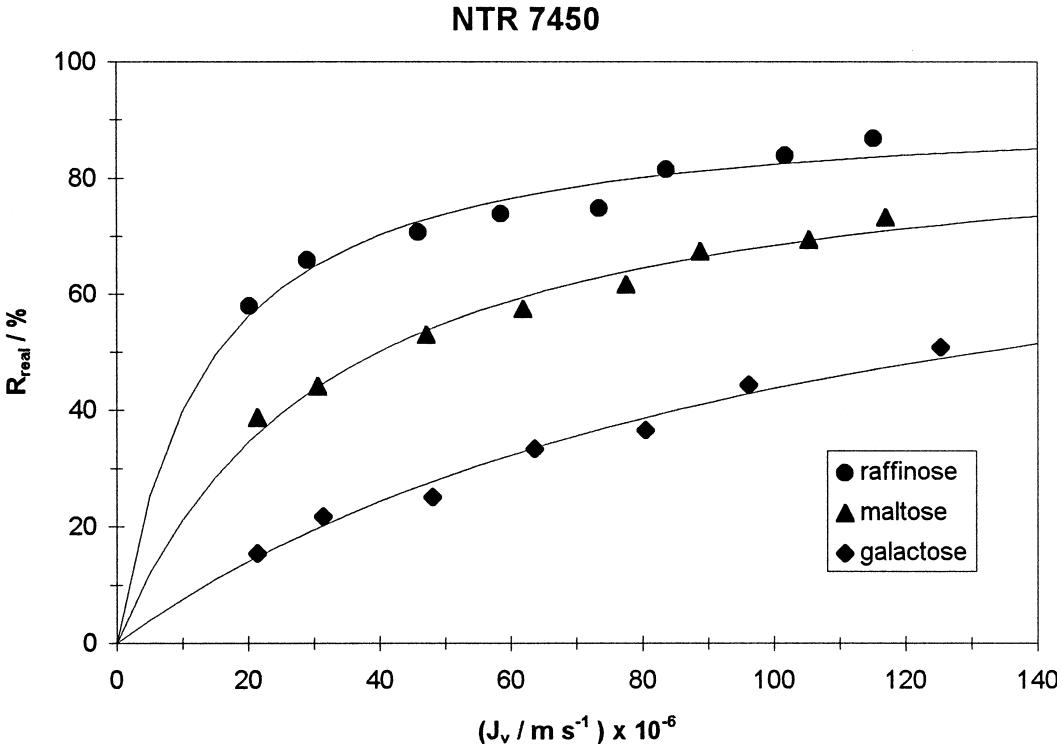

FIG. 2 The retention of three saccharides as a function of the permeate flux for the NTR7450 membrane. The full lines are the result of a best fit using Eqs. (9) and (10).

MARCEL DEKKER, INC.
270 Madison Avenue, New York, New York 10016

NTR7450. For NF40 and UTC20 only the data for galactose were used to determine the pore radius, giving a value of 0.42 nm for NF 40 and of 0.41 nm for UTC20. Because of the high saccharide retentions, these pore radii for NF40 and for UTC20 should only be considered as approximate.

A single value of $\Delta x/A_k$ could not be determined for CA30 and NTR7450. Table 3 shows that no constant values were obtained by the model, but for the CA30 membrane it appears that the values for $\Delta x/A_k$ decrease with increasing solute size. This phenomenon has been found before (3, 20–22) and seems to be caused by a too simple representation of the membrane structure. It was postulated (21) that the structure of this type of membrane consists of pores which are interconnected, so that small solutes have greater $\Delta x/A_k$ values than larger solutes because of their longer transport paths due to the ability to permeate through the smaller pores of the network. In this paper the influence of the size of the solute on the value for $\Delta x/A_k$ will not be taken into account. Instead, the value for $\Delta x/A_k$ that will be used to analyze salt rejection data is calculated using the Hagen–Poiseuille equation; this means that the solute size is neglected in calculation of $\Delta x/A_k$. The values for $\Delta x/A_k$ are calculated from the last column of Table 2, using the average pore radii obtained from uncharged solutes experiments. These values for the pore radius and for the ratio of the membrane thickness to the porosity will be used to analyze salt rejection data and are summarized in Table 4 for the four membranes.

Single Salt Solutions

The retention of single salt solutions was determined for the four nanofiltration membranes. A complete set of experiments was carried out for NaCl, Na_2SO_4, $MgCl_2$, and $MgSO_4$. Retention was measured as a function of the flux at different salt concentrations.

TABLE 3
Result of Best Fit for Uncharged Solutes Using the DSPM Model. The Pore Radius and the Ratio of the Membrane Thickness to the Porosity Were Fitted Independently

	CA30		NTR7450		NF40		UTC20	
Solute	r_p (nm)	$\Delta x/A_k$ (μm)	r_p (nm)	$\Delta x/A_k$ (μm)	r_p (nm)	$\Delta x/A_k$ (μm)	r_p (nm)	$\Delta x/A_k$ (μm)
Galactose	0.95	5.75	0.55	0.03	0.42	0.82	0.41	0.08
Maltose	0.94	2.99	0.71	0.09				
Raffinose	0.93	0.89	0.80	0.08				

MARCEL DEKKER, INC.
270 Madison Avenue, New York, New York 10016

TABLE 4
Membrane Characteristics Used to Analyze Salt Rejection Data. The Effective Pore Radius Is Determined from Uncharged Solutes Experiments (average value), and the Ratio of the Effective Thickness to the Porosity is Calculated from Pure Water Permeability Data Using This Effective Pore Radius

Membrane	r_p (nm)	$\Delta x/A_k$ (μm)
CA30	0.94	6.8
NTR7450	0.69	1.0
NF40	0.42	0.95
UTC20	0.41	0.34

For each set of experiments the retention versus flux was fitted by the DSPM model. Besides physical data of the ions (such as diffusion coefficient and ion radius), three input parameters are needed: the pore radius, the ratio of the membrane thickness to the porosity, and the membrane charge density. Values for the effective pore radius and for the ratio of the effective thickness to the porosity were taken from Table 4. The model then evaluates the membrane charge density in order to obtain a best fit of the experimental retentions. The experimental results and the modeling results will be discussed for each membrane separately.

CA30

At concentrations of 10–200 meq/L, the experimental points of Fig. 3 show that very little NaCl is retained by the CA30 membrane. The retention is almost independent of the NaCl concentration and increases with increasing water flux. For Na_2SO_4 the retentions are higher and a decrease is found with increasing concentrations. At concentrations above 50 meq/L the retention is almost independent of the concentration but increases with the flux to ca. 40% at the highest measured flux value (at 20 bar). The $MgCl_2$ retention is somewhat higher than for NaCl and is also nearly independent of the feed concentration. The retention for $MgSO_4$ is higher than for $MgCl_2$, and $MgSO_4$ is 60% retained at the highest measured flux.

The idea of a weakly negative membrane charge in the case of a cellulose acetate material is in accordance with the experimental findings: salt retentions are rather low, and sulfate salts are better retained than chloride salts. However, no explanation is found for the fact that $MgCl_2$ is better retained than NaCl. On the basis of Donnan exclusion, the opposite is expected in the case of a negative membrane charge (16).

MARCEL DEKKER, INC.
270 Madison Avenue, New York, New York 10016

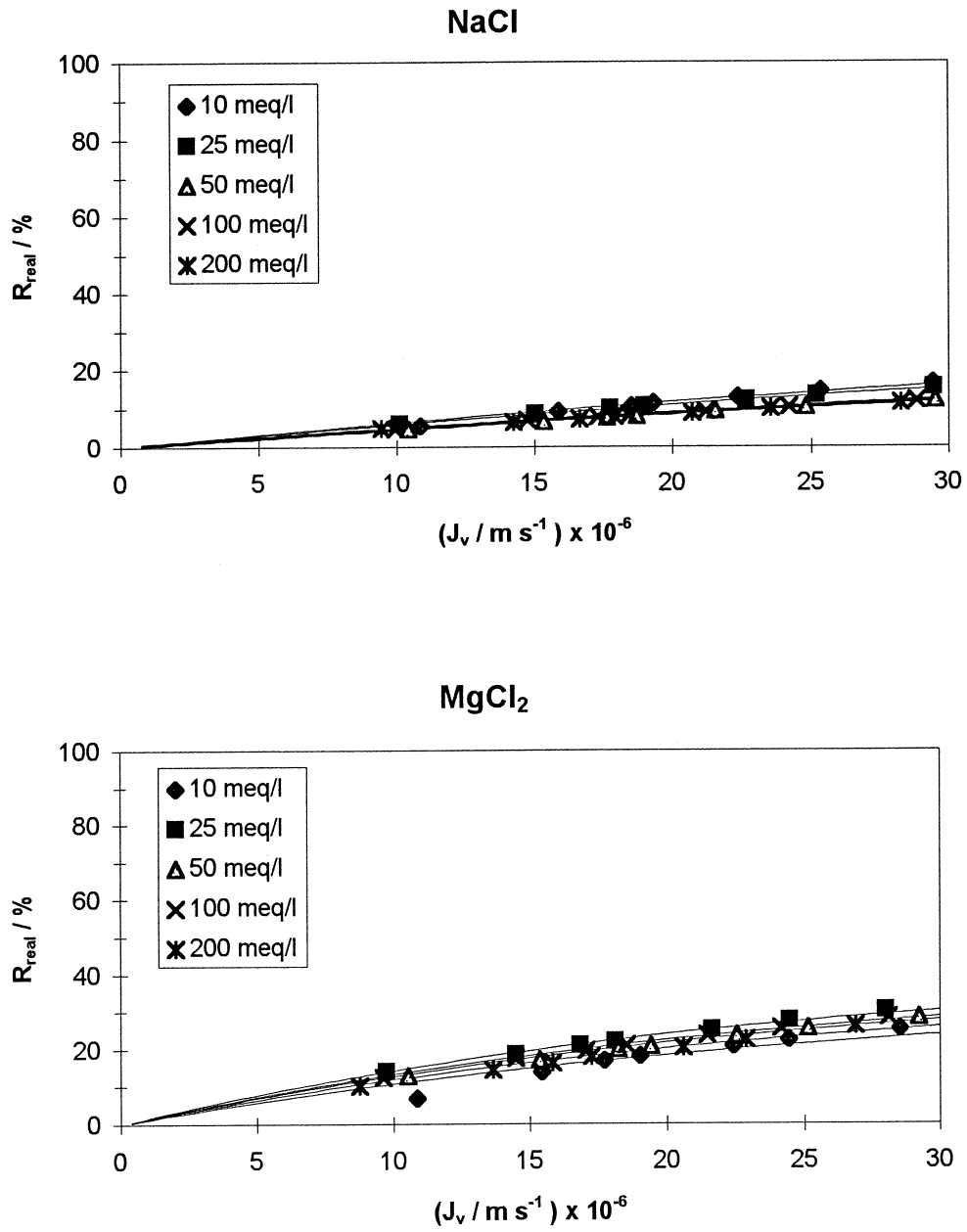

FIG. 3 The retention of single salt solutions as a function of the permeate flux at different salt concentrations for the CA30 membrane.

Salt retentions were fitted by the DSPM model. The full lines of Fig. 3 are the model predictions. It can be seen from Fig. 3 that the experimental data could be fitted very well. The values for the membrane charge density thus obtained are given in Fig. 4. It appears that the charge density is not constant but depends very much on the salt and on the salt concentration, and can be de-

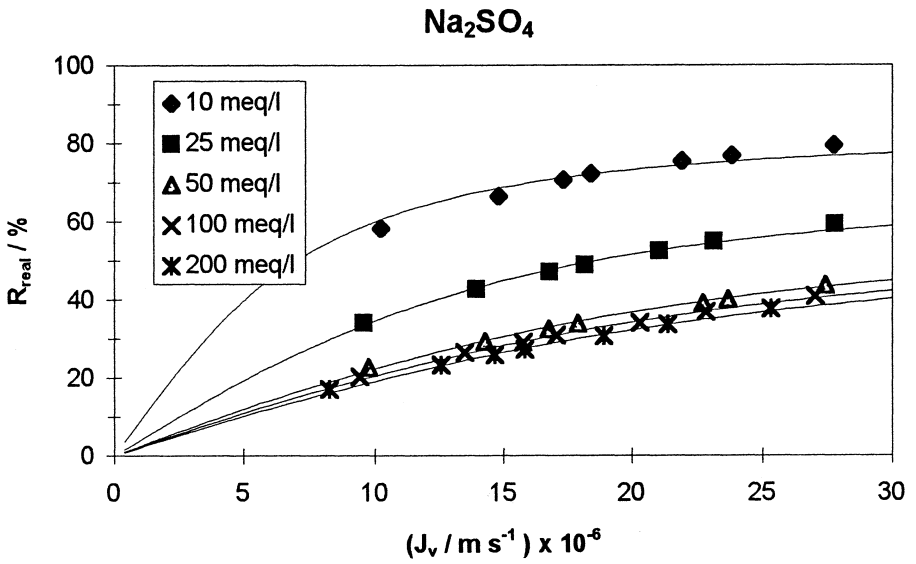

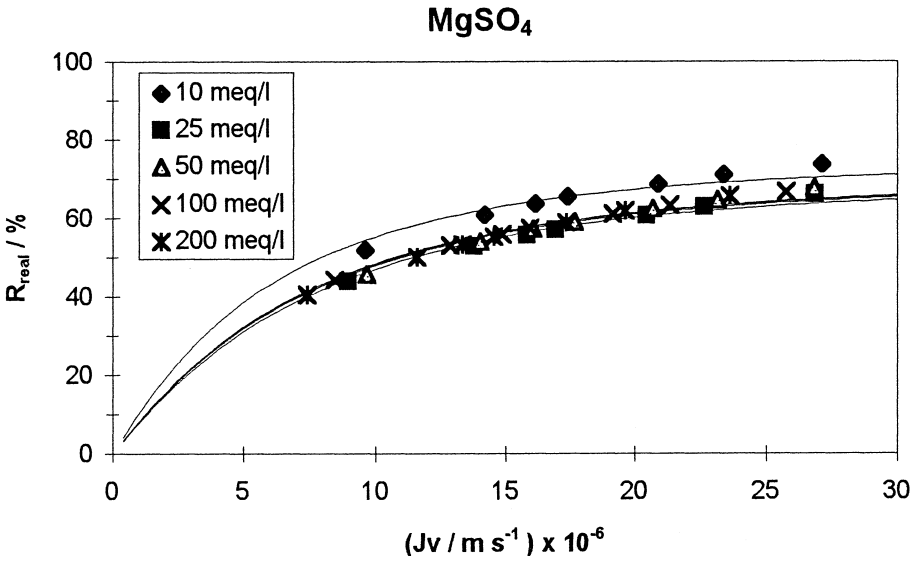

FIG. 3 Continued

scribed by linear isotherms. This phenomenon was found before, and it was ascribed to ion adsorption (3, 23, 24) on the membrane material. In the case of, e.g., NaCl, adsorption of chloride ions would then lead to a more negative membrane charge at higher electrolyte concentrations.

Figure 4 also shows that the membrane charge becomes positive for the two magnesium salts. This suggests that each individual ion could make its indi-

MARCEL DEKKER, INC.
270 Madison Avenue, New York, New York 10016

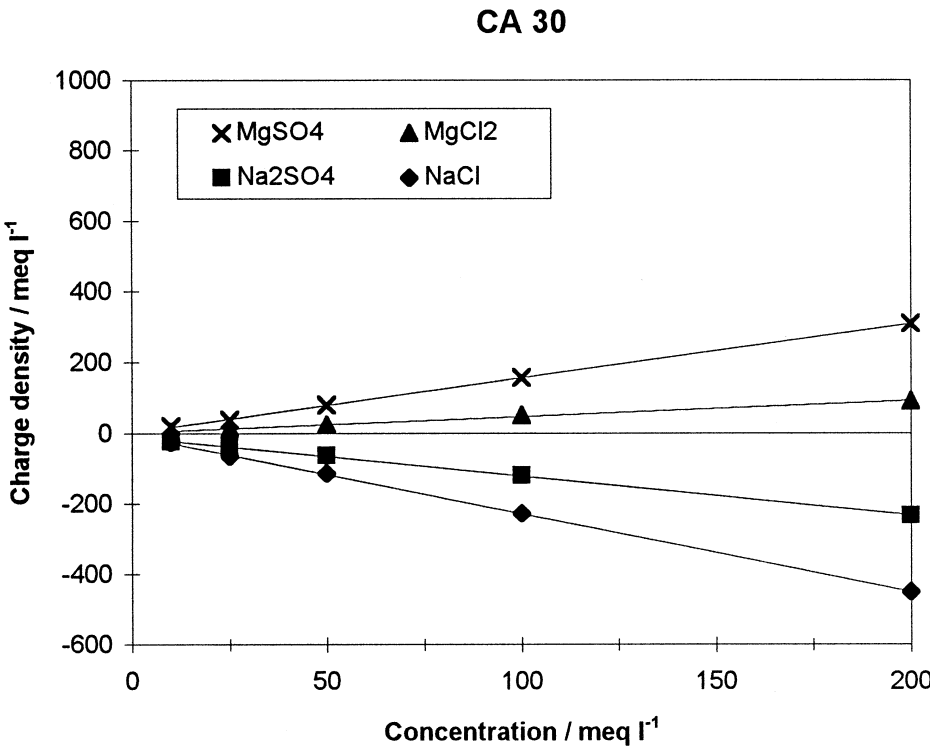

FIG. 4 Effective charge density as a function of the salt concentration for the CA30 membrane. Linear isotherms for 10–200 meq/L:

NaCl	$X = -2.23C^0 - 5.84$
Na_2SO_4	$X = -1.08C^0 - 15.83$
$MgCl_2$	$X = 0.45C^0 + 1.60$
$MgSO_4$	$X = 1.53C^0 + 1.85$

vidual contribution to the membrane charge by means of adsorption. In that way the presence of magnesium could alter the sign of the membrane charge so that the membranes become positively charged. This could explain the fact that $MgCl_2$ is better retained than NaCl: magnesium is the co-ion (= ion with the same charge sign as the membrane charge) in the case of $MgCl_2$ and has a higher valence than chloride, which is the co-ion in the case of NaCl. On the basis of Donnan exclusion, a higher co-ion valence causes a higher salt retention.

Some additional calculations were made to study the mechanism of membrane charging. It could be suggested that for a membrane in contact with a single salt solution, each ion makes its own contribution to the membrane charge and that the overall membrane charge density could be represented by one isotherm for the salt. For CA30 the membrane charge density for solutions of $MgSO_4$ was calculated by adding the values for Na_2SO_4 to the values for $MgCl_2$ and subtracting the values for NaCl. The calculated values for the

membrane charge density show very good agreement with the values directly obtained through evaluation of rejection data for the whole concentration range (see Table 5). This shows that for the CA30 membrane the membrane charge density can be calculated by adding the contributions of individual ions, which should be very promising for the prediction of the membrane performance for salt mixtures.

NTR7450

The NTR7450 membrane is composed of a sulfonated polyethersulfone layer, with a high negative charge at neutral pH. Salt retentions are high for NaCl and for Na_2SO_4 but decrease substantially with increasing feed concentration (Fig. 5). The lowest retention is found for $MgCl_2$. Evaluation of the membrane charge density shows that for this membrane the charge also depends on the salt and its concentration (Fig. 6). The charge density can be described by linear isotherms.

It has to be mentioned that ion adsorption is not expected to be the major charging mechanism here as the membrane carries a strong inherent negative charge. Nevertheless, a positive membrane charge is again found with solutions of $MgSO_4$ while the membrane appears to be more or less neutral with solutions of $MgCl_2$. This seems to be caused by adsorption of magnesium ions.

Calculations were made in order to predict the membrane charge density for $MgSO_4$ by adding values for Na_2SO_4 to values for $MgCl_2$ and subtracting the values for NaCl, but the charge density was overpredicted (see Table 6). Thus, addition of the individual contributions of each ion to obtain the overall membrane charge density cannot be applied to this membrane.

TABLE 5
Comparison of the Charge Density of the CA30 Membrane for Solutions of $MgSO_4$

Concentration (meq/L)	XNaCl[a] (meq/L)	$X$$Na_2SO_4$[a] (meq/L)	$X$$MgCl_2$[a] (meq/L)	$X$$MgSO_4$[a] (meq/L)	$X$$MgSO_4$[b] (meq/L)
10	−27.4	−23.6	4.1	19.4	7.9
25	−65.8	−40.3	13.2	37.3	38.7
50	−113.1	−63.6	24.1	77.7	73.6
100	−228.1	−121.5	49.7	156.2	156.3
200	−451.5	−234.2	90.0	307.3	307.3

[a] Directly obtained from rejection data with DSPM.
[b] Calculated by adding the values for Na_2SO_4 to the values for $MgCl_2$ and subtracting the values for NaCl.

MARCEL DEKKER, INC.
270 Madison Avenue, New York, New York 10016

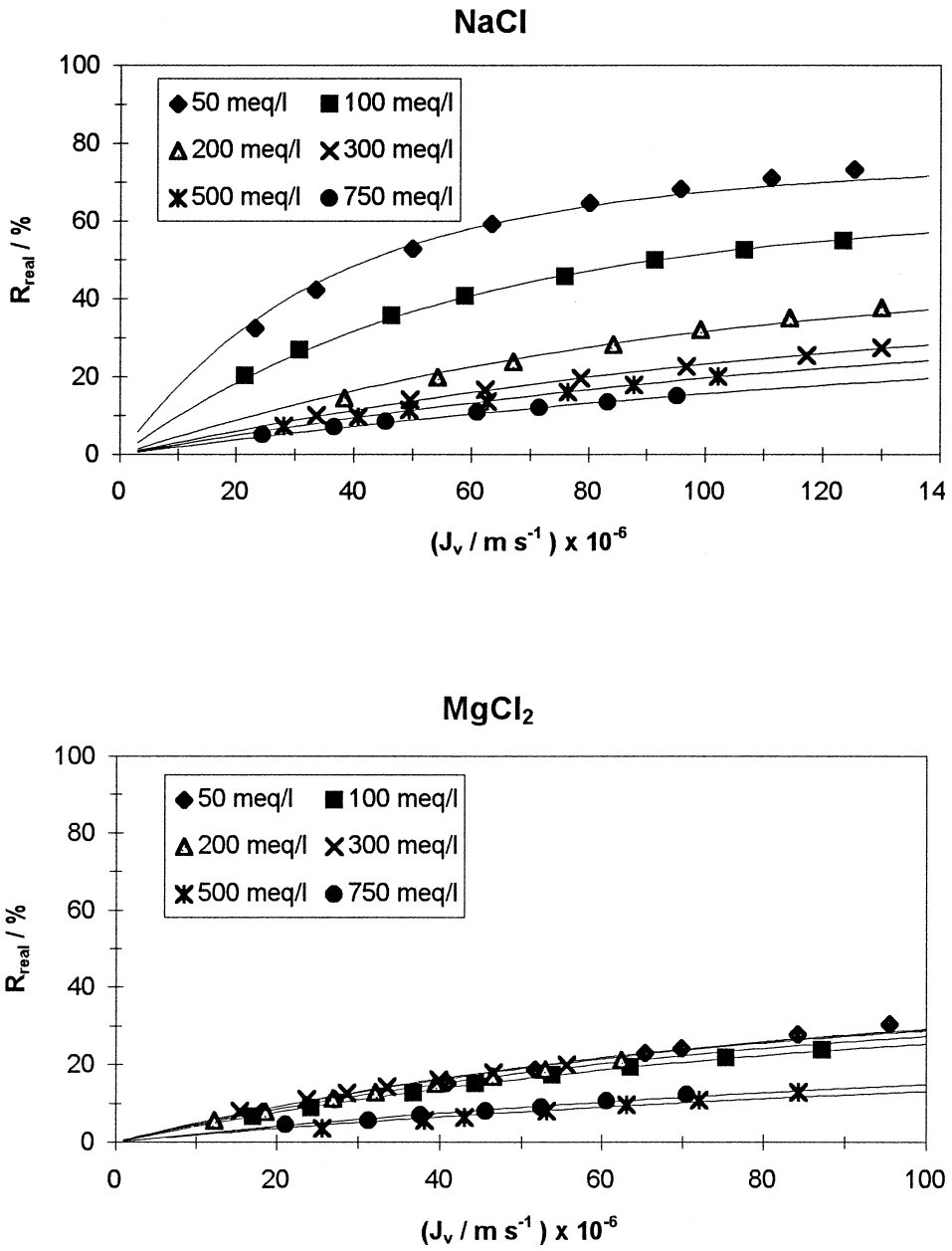

FIG. 5 The retention of single salt solutions as a function of the permeate flux at different salt concentrations for the NTR7450 membrane.

NF40

Salt retentions at a transmembrane pressure of 20 bar for the NF40 membrane, are given in Table 7 at different feed concentrations. A salt retention between 64 and 28% is found for NaCl but all other salts are almost completely retained, even at high concentrations. At increasing concentrations the perme-

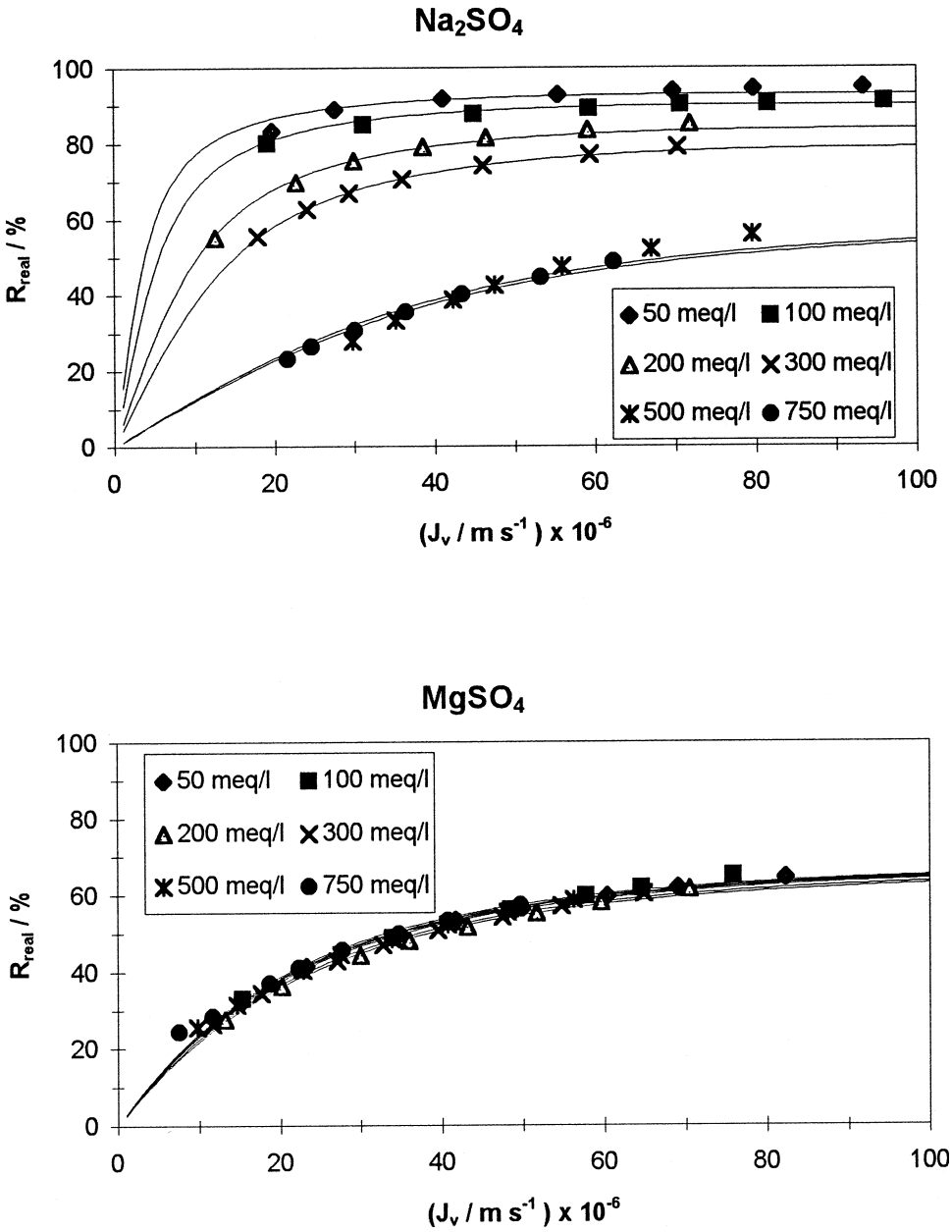

FIG. 5 Continued

ate flux at 20 bar decreased very much due to a higher osmotic pressure at the membrane. The high retention of multivalent ions is a typical characteristic of nanofiltration membranes. Due to the very small pore radius, the retention is mainly determined by the steric hindrance of the ion at the entrance of a membrane pore, especially for magnesium (Stokes radius of 0.35 nm) and for sulfate (0.23 nm) and to a lesser extent for sodium (0.18 nm) and for chloride (0.12 nm) (15).

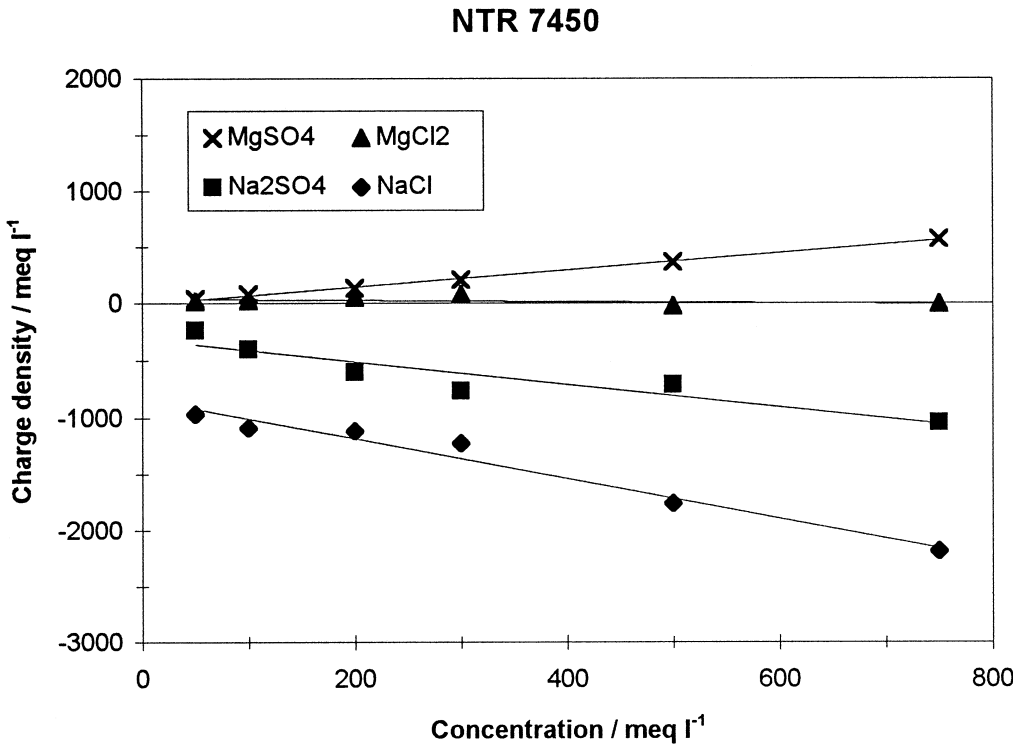

FIG. 6 Effective charge density as a function of salt concentration for the NTR7450 membrane. Linear isotherms for 50–750 meq/L:

NaCl	$X = -1.76C^0 - 832.79$
Na_2SO_4	$X = -0.98C^0 - 312.60$
$MgCl_2$	$X = -0.06C^0 + 40.79$
$MgSO_4$	$X = 0.76C^0 - 9.27$

TABLE 6
Comparison of the Charge Density of the NTR7450 Membrane for Solutions of $MgSO_4$

Concentration (meq/L)	XNaCl[a] (meq/L)	$X$$Na_2SO_4$[a] (meq/L)	$X$$MgCl_2$[a] (meq/L)	$X$$MgSO_4$[a] (meq/L)	$X$$MgSO_4$[b] (meq/L)
50	−967.0	−240.0	13.6	36.9	740.6
100	−1092.0	−400.0	20.6	74.6	712.6
200	−1119.0	−598.0	48.1	135.1	569.1
300	−1228.0	−760.2	79.8	208.5	547.6
500	−1759.0	−705.7	−21.3	362.3	1032.0
750	−2184.0	−1042.0	−1.6	570.7	1140.4

[a] Directly obtained from rejection data with DSPM.
[b] Calculated by adding the values for Na_2SO_4 to the values for $MgCl_2$ and subtracting the values for NaCl.

MARCEL DEKKER, INC.
270 Madison Avenue, New York, New York 10016

TABLE 7
Salt Retention (%) at 20 bar for the NF40 Membrane

Concentration (meq/L)	NaCl	Na_2SO_4	$MgCl_2$	$MgSO_4$
50	64	99	99	100
100	57	99	99	100
200	49	99	99	100
300	43	99	98	97
500	35	99		100
750	28			

Application of the DSPM model to fit the experimental results was only carried out for NaCl and showed a linear isotherm for concentrations between 50 and 750 meq/L: $X = -5.84C^0 - 488.61$. For the other three salt solutions, no best fit calculations were carried out.

UTC20

Salt retentions at a transmembrane pressure of 20 bar for the UTC20 membrane, are given in Table 8 at different feed concentrations. A retention between 75 and 26% is found for NaCl; all other salts are almost completely retained at concentrations below 200 meq/L. The salt retentions are more concentration dependent than for the NF40 membrane. The permeate flux at 20 bar also decreased very much at increasing concentration due to the osmotic pressure effect.

Application of the DSPM model to fit the experimental results was only carried out for NaCl and showed a linear isotherm for concentrations between 50 and 750 meq/L: $X = -3.79C^0 - 860.82$.

TABLE 8
Salt Retention (%) at 20 bar for the UTC20 Membrane

Concentration (meq/L)	NaCl	Na_2SO_4	$MgCl_2$	$MgSO_4$
50	75	99	97	98
100	64	99	96	98
200	54	95	94	97
300	45	96	91	97
500	35	96	74	97
750	26	84	51	96

MARCEL DEKKER, INC.
270 Madison Avenue, New York, New York 10016

CONCLUSIONS

The DSPM model was used to characterize four commercial nanofiltration membranes in terms of an effective pore radius and the ratio of an effective membrane thickness to the porosity. For membranes with a small pore radius (0.42 nm for NF40 and 0.41 nm for UTC20), the salt retention was found to be very high for Na_2SO_4, $MgCl_2$, and $MgSO_4$, and moderate for NaCl, a typical characteristic of nanofiltration membranes. For CA30 and NTR7450, membranes which were found to have larger pore radii, the salt retention was much lower. The salt retention can be explained in terms of charge and steric interactions between ion and membrane.

The retention of single salt solutions was analyzed by the DSPM model to evaluate the membrane charge density. The general patterns were similar for all four membranes. The charge density was very much dependent on the salt and on its concentration and could even change its sign. A possible explanation is that this is caused by interactions between free ions in solution and the membrane, where each individual ion makes its contribution to the membrane charge by means of adsorption. More insight into the adsorption mechanism is required in order to take these interactions into account and to allow predictions of the membrane performance.

LIST OF SYMBOLS

A_k	porosity of the membrane
c_i	concentration in the membrane ($mol \cdot m^{-3}$)
$C_{i,m}$	concentration on the feed side of the membrane ($mol \cdot m^{-3}$)
$C_{i,p}$	concentration in the permeate ($mol \cdot m^{-3}$)
C^0	bulk solution concentration ($mol \cdot m^{-3}$)
d_h	equivalent hydraulic diameter (m)
$D_{i,p}$	hindered diffusivity ($m^2 \cdot s^{-1}$)
$D_{i,\infty}$	bulk diffusivity ($m^2 \cdot s^{-1}$)
F	Faraday constant ($C \cdot mol^{-1}$)
G	hydrodynamic lag coefficient
I_c	current density ($A \cdot m^{-2}$)
j_i	ion flux ($mol \cdot m^{-2} \cdot s^{-1}$)
J_v	volume flux (based on membrane area) ($m \cdot s^{-1}$)
J_w	water flux (based on membrane area) ($m \cdot s^{-1}$)
k	mass transfer coefficient ($m \cdot s^{-1}$)
K^{-1}	hydrodynamic enhanced drag coefficient
$K_{i,c}$	hindrance factor for convection
$K_{i,d}$	hindrance factor for diffusion
Pe_m	Peclet number
ΔP	applied pressure difference (bar)

MARCEL DEKKER, INC.
270 Madison Avenue, New York, New York 10016

r_p	effective pore radius (m)
R	gas constant ($J \cdot mol^{-1} \cdot K^{-1}$)
R_{real}	real rejection
Re	Reynolds number
Sc	Schmidt number
Sh	Sherwood number
T	absolute temperature (K)
V	solute velocity ($m \cdot s^{-1}$)
x	distance normal to membrane (m)
Δx	effective membrane thickness (m)
X	effective membrane charge density ($mol \cdot m^{-3}$)
z_i	valence of ion
ϕ	steric partitioning term
λ	ratio of ionic or solute radius to pore radius
μ	viscosity of solution (Pa·s)
ψ	electric potential in axial direction (V)
$\Delta_{\psi D}$	Donnan potential (V)

ACKNOWLEDGMENTS

This research was financed with a fellowship from “het Vlaams Instituut voor de bevordering van het wetenschappelijk-technologisch onderzoek in de industrie (IWT).” The F.W.O. (Fonds voor Wetenschappelijk Onderzoek - Vlaanderen) is gratefully acknowledged for its financial support. The UK BBSRC is also thanked for its support of this work.

REFERENCES

1. L. P. Raman, M. Cheryan, and N. Rajagopalan, “Consider Nanofiltration for Membrane Separations,” *Chem. Eng. Prog.*, *90*, 68–74 (1994).
2. M. Mulder, *Basic Principles of Membrane Technology*, 2nd ed., Kluwer Academic Publishers, Dordrecht, 1996.
3. W. R. Bowen, A. W. Mohammad, and N. Hilal, “Characterisation of Nanofiltration Membranes for Predictive Purposes—Use of Salts, Uncharged Solutes and Atomic Force Microscopy,” *J. Membr. Sci.*, *126*, 91–105 (1997).
4. W. R. Bowen and H. Mukhtar, “Characterisation and Prediction of Separation Performance of Nanofiltration Membranes,” *Ibid.*, *112*, 263–274 (1996).
5. X. L. Wang, T. Tsuru, S. Nakao, and S. Kimura, “Electrolyte Transport through Nanofiltration Membranes by the Space-Charge Model and the Comparison with Teorell–Meyer–Sievers Model,” *Ibid.*, *103*, 117–133 (1995).
6. W. R. Bowen and A. W. Mohammad, “Diafiltration by Nanofiltration: Prediction and Optimization,” *AIChE J.*, *44*, 1799–1812 (1998).
7. W. R. Bowen and A. O. Sharif, “Transport through Microfiltration Membranes: Particle Hydrodynamics and Flux Reductions,” *J. Colloid Interface Sci.*, *168*, 414–421 (1994).
8. W. M. Deen, “Hindered Transport of Large Molecules in Liquid-Filled Pores,” *AIChE J.*, *33*, 1409–1425 (1987).

9. G. Hagmeyer and R. Gimbel, "Modelling the Salt Rejection of Nanofiltration Membranes for Ternary Ion Mixtures and for Single Salts at Different pH Values," *Desalination*, *117*, 247 (1998).
10. J. R. Bontha and P. N. Pintauro, "Water Orientation and Ion Solvation Effects during Multicomponent Salt Partitioning in a Nation Cation Exchange Membrane," *Chem. Eng. Sci.*, *49*, 3835 (1994).
11. M. S. Hall, V. M. Starov, and D. R. Lloyd, "Reverse Osmosis of Multicomponent Electrolyte Solutions. Part I. Theoretical Development," *J. Membr. Sci.*, *128*, 23–37 (1997).
12. R. Simons, "Trace Element Removal from Ash Dam Waters by Nanofiltration and Diffusion Dialysis," *Desalination*, *89*, 325–341 (1993).
13. P. Eriksson, "Nanofiltration Extends the Range of Membrane Filtration," *Environ. Prog.*, *7*, 58–62 (1988).
14. R. J. Petersen, "Composite Reverse Osmosis and Nanofiltration Membranes," *J. Membr. Sci.*, *83*, 81–150 (1993).
15. J. Schaep, "Nanofiltration for the Removal of Ionic Components from Water," Ph.D. Thesis, Katholieke Universiteit Leuven, Heverlee, Belgium, 1999.
16. J. Schaep, B. Van der Bruggen, C. Vandecasteele, and D. Wilms, "Influence of Ion Size and Charge in Nanofiltration," *Sep. Purif. Technol.*, *14*, 155–162 (1998).
17. P. A. Schweitzer, *Handbook of Separations Techniques for Chemical Engineers*, 2nd ed., McGraw-Hill, New York, NY, 1988.
18. J. S. Newman, *Electrochemical Systems*, 2nd ed., Prentice-Hall, Englewood Cliff, NJ, 1991.
19. M. Dubois, K. A. Gilles, J. K. Hamilton, P. A. Rebers, and F. Smith, "Colorimetric Method for Determination of Sugars and Related Substances," *Anal. Chem.*, *28*, 350–356 (1956).
20. S. Sarrade, G. M. Rios, and M. Carles, "Dynamic Characterization and Transport Mechanisms of Two Inorganic Membranes for Nanofiltration," *J. Membr. Sci.*, *97*, 155–166 (1994).
21. S. Nakao and S. Kimura, "Analysis of Solutes Rejection in Ultrafiltration," *J. Chem. Eng. Jpn.*, *14*, 32–37 (1981).
22. S. Nakao and S. Kimura, "Models of Membrane Transport Phenomena and Their Applications for Ultrafiltration Data," *Ibid.*, *15*, 200–205 (1982).
23. J. M. M. Peeters, "Characterization of Nanofiltration Membranes," Ph.D. Thesis, University of Twente, Enschede, Netherlands, 1997.
24. X. L. Wang, T. Tsuru, M. Togoh, S. Nakao, and S. Kimura, "Evaluation of Pore Structure and Electrical Properties of Nanofiltration Membranes," *J. Chem. Eng. Jpn.*, *28*, 186–192 (1995).

Received by editor December 7, 1998
Revision received March 1999

Request Permission or Order Reprints Instantly!